arXiv:1912.04309v2 [hep-ph] 14 Sep 2020

FTUAM-19-24
IFT-UAM/CSIC-19-162

Physics potential of the ESSνSB

M. Blennow,[a,b] E. Fernandez-Martinez,[a] T. Ota[a] and S. Rosauro-Alcaraz[a]

[a] *Departamento de Física Teórica and Instituto de Física Teórica, IFT-UAM/CSIC, Universidad Autónoma de Madrid, Cantoblanco, 28049, Madrid, Spain*
[b] *Department of Physics, School of Engineering Sciences, KTH Royal Institute of Technology, AlbaNova University Center, Roslagstullsbacken 21, SE–106 91 Stockholm, Sweden*

Abstract

The ESSνSB project proposes to base a neutrino "Super Beam" of unprecedented luminosity at the European Spallation Source. The original proposal identified the second peak of the oscillation probability as the optimal to maximize the discovery potential to leptonic CP violation. However this choice reduces the statistics at the detector and penalizes other complementary searches such as the determination of the atmospheric oscillation parameters, particularly the octant of θ_{23} as well as the neutrino mass ordering. We explore how these shortcomings can be alleviated by the combination of the beam data with the atmospheric neutrino sample that would also be collected at the detector. We find that the combination not only improves very significantly these drawbacks, but also enhances both the CP violation discovery potential and the precision in the measurement of the CP violating phase, for which the facility was originally optimized, by lifting parametric degeneracies. We then reassess the optimization of the ESSνSB setup when the atmospheric neutrino sample is considered, with an emphasis in performing a measurement of the CP violating phase as precise as possible. We find that for the presently preferred value of $\delta \sim -\pi/2$, shorter baselines and longer running time in neutrino mode would be optimal. In these conditions, a measurement better than 14° would be achievable for any value of the θ_{23} octant and the mass ordering. Conversely, if present and next generation facilities were not able to discover CP violation, longer baselines and more even splitting between neutrino and neutrino modes would be preferable. These choices would allow a 5σ discovery of CP violation for around a 60% of the possible values of δ and to determine its value with a precision around 6° if it is close to 0 or π.

1 Introduction

After the discovery of a non-zero θ_{13} [1–5] the emerging picture from the last decades of neutrino oscillation searches consolidates a structure for the PMNS matrix [6–10] describing lepton flavour mixing strikingly different from its CKM counterpart in the quark sector, making the Standard Model flavour puzzle even more intriguing. Far from the hierarchical structure described through the tiny mixing angles of the CKM, large mixing angles characterize the lepton mixing. The "atmospheric" mixing angle θ_{23} is presently compatible with maximal mixing as well as with a large but non-maximal value in either the first or the second octant. Similarly, the "solar" mixing angle θ_{12} is around 33° and only $\theta_{13} \sim 8-9^\circ$ is relatively small and its value is still comparable in magnitude to the Cabibbo angle, the largest in the CKM. The large mixing opens the window to the present and next generation of neutrino oscillation experiments to tackle new questions that could provide answers to fundamental open problems.

Present experiments such as T2K [11, 12] and NOνA [13] have started to provide the first hints on the potentially CP-violating phase δ. The discovery of the violation of the particle-antiparticle symmetry in the lepton sector would be extremely suggestive, given that CP-violation is a necessary ingredient to explain the matter over antimatter excess to which we owe our existence and that the CKM contribution has been shown to be insufficient [14,15] for this purpose. Similarly, present neutrino oscillation experiments already show some preference for normal ordering (positive Δm^2_{31}) with respect to inverted ordering. This parameter is a fundamental input to combine with the searches for the neutrinoless double beta decay process in order to probe the Majorana nature of neutrinos. Finally, present experiments as well as their successors T2HK [16] and DUNE [17] will also provide even more precise measurements of the oscillation parameters that could hold the key to discriminate among different flavour models addressing the flavour puzzle.

The European Spallation Source (ESS) at Lund provides an opportunity to build a new-generation, long-baseline neutrino oscillation experiment with an unprecedented neutrino luminosity through an upgrade of the ESS Linac [18]. Its 2.5 GeV protons would lead to a rather low energy neutrino flux, between 200 and 600 MeV. This energy range is very well suited for a water Cerenkov detector of the MEMPHYS type [19, 20]. In Ref. [18] a green-field study optimizing the physics reach to leptonic CP-violation was performed for this ESS neutrino Super-Beam facility (ESSνSB). Interestingly, the outcome of this optimization, as well as follow-up studies [21–23], was that the best baseline at which to study the neutrino beam from the ESS facility at a MEMPHYS-type detector would be between 400 and 600 km. Two candidate mines that could host the detector were identified: Garpenberg at 540 km and Zinkgruvan at 360 km from the ESS site. This choice makes the ESSνSB design unique, as the neutrino flux observed by the detector mainly corresponds to the second maximum of the $\nu_\mu \to \nu_e$ oscillation probability, with a marginal contribution of events at the first oscillation peak.

For the value of $\theta_{13} = 8.6^\circ$ currently preferred [24] by Daya Bay [25] and RENO [26], the "atmospheric" term of the $\nu_\mu \to \nu_e$ oscillation probability [27], which is governed by oscillations driven by the large frequency Δm^2_{31} and with an amplitude $\sin^2 2\theta_{13}$, dominates over the sub-leading "solar" term driven by Δm^2_{21} with amplitude $\sin^2 2\theta_{12}$ at the first oscillation maximum. Thus, the interference between the two, which is the only term dependent on the yet unknown CP-violating phase δ, will also be a sub-leading contribution to the full oscillation probability at the first peak and potentially hidden by systematic uncertainties.

Conversely, at the second oscillation maximum the slower "solar" oscillation has had more time to develop and thus the CP-violating interference term can give a significant contribution to the oscillation probability, thus increasing the sensitivity to CP violation [28].

The price to pay in order to observe the oscillation probability at its second maximum is high. Despite this being the optimal choice to maximize the dependence of the oscillation probability on the leptonic CP violating phase, the ratio of the oscillation baseline to the neutrino energy (L/E) needs to be a factor 3 larger compared to the first maximum. This implies roughly an order of magnitude less statistics than if the experiment had been designed at the first peak. Indeed, the neutrino flux decreases with L^{-2} from the beam divergence and the neutrino cross section and beam collimation increase with the neutrino energy. Despite the unprecedented neutrino luminosity from the upgraded ESS linac and the megaton-class MEMPHYS detector, only around 100 signal events for each beam polarity would be accumulated after 10 years data taking (2 years in neutrinos and 8 years in antineutrinos) at the 540 km Garpenberg baseline (see Fig. 7 of Ref. [18]). Conversely, the 360 km Zinkgruvan baseline has a 2.25 times larger neutrino flux. However, the neutrino spectrum for this baseline is rather centered at the first oscillation minimum while the first and second peaks are sampled by the high and low energy tails respectively. Overall this gives similar statistics at the second oscillation maximum when compared to the Garpenberg option, but also some additional statistics at the first peak and in between.

For the ESSνSB the increased dependence on the CP violating phase of the probability is well worth the loss of precious neutrino events at the second maximum. Indeed, it could provide unprecedented discovery potential to leptonic CP-violation or the most precise measurement of the corresponding phase after discovery, which could be instrumental in tackling the flavour puzzle. Moreover, as pointed out in Ref. [28] and as we will elaborate in later sections, this choice also makes the physics reach much more resilient against unexpected sources of systematic errors, since the signal, while small, has a leading dependence on the unknown parameters. Conversely, statistics will be the bottleneck of the ESSνSB physics reach and thus longer periods of data taking would greatly increase its capabilities.

On the other hand, other potential oscillation searches, different from the CP violation search, will be negatively impacted by the choice of the second oscillation maximum baseline. In particular the sensitivity to the octant of θ_{23} is severely reduced by this choice. Indeed, this measurement mainly relies on the "atmospheric" term of the oscillation probability, which is leading at the first maximum instead, together with θ_{13} information from reactor measurements and Δm^2_{31} and $\sin^2 2\theta_{23}$ from ν_μ disappearance. Similarly the ν_μ disappearance data and hence the precise determination of Δm^2_{31} and $\sin^2 2\theta_{23}$ are negatively affected by the choice of the second oscillation maximum. The lack of knowledge on the octant of θ_{23} can lead to "octant degeneracies" [29] that in turn somewhat limit the CP discovery potential of the ESSνSB [30]. The sensitivity to the mass ordering is also limited at the ESSνSB given the small matter effects from the low energy and short baseline. However, since these matter effects are small, the resulting "sign degeneracies" [31] do not compromise the sensitivity to δ of the facility [18, 30].

A very effective and convenient way of increasing both the octant and mass ordering sensitivity of a neutrino Super Beam experiment is to combine the signal from the neutrino beam with the huge atmospheric neutrino sample that can be collected at such a detector [32, 33]. In the case of the ESSνSB this combination is particularly synergistic. Indeed, the atmospheric neutrino sample can provide not only significantly increased sensitivity to the octant and the mass ordering to solve parametric degeneracies, but also improved precision

to Δm^2_{31} and $\sin^2 2\theta_{23}$ which is otherwise one of the main drawbacks of the setup.

In this work we will combine the observation of the ESSνSB flux tuned for the second maximum of the ν_e appearance probability with the complementary atmospheric neutrino data, more strongly dominated by the first maximum and ν_μ disappearance, and characterized by stronger matter effects. We will explore how the physics reach of the facility improves when beam data is considered together with the atmospheric neutrino sample and then review the optimization of the ESSνSB facility using both data sets. Finally, we will discuss which sources of systematic errors among the ones considered impact the final sensitivity more significantly.

This paper is organized as follows. In Section 2 we discuss the peculiarities of the neutrino oscillation probability and the appearance of parametric degeneracies when observing at the second oscillation maximum. In Section 3 we describe the experimental setup considered and the details of the numerical simulations performed. Section 4 describes the results of the simulations and in Section 5 we present our conclusions and summarize our work.

2 Measurements at the second oscillation peak

The determination of the oscillation parameters at beam experiments is, in general, hindered by the appearance of degenerate solutions, cf. e.g., Refs. [34–38]. These degeneracies have been extensively studied for the experimental setups of T2HK [39–44] and DUNE [17, 39, 43, 45–56] (and also their combination [57, 58]). As stated in Section 1, the L/E range which the ESSνSB focuses on is different from those of other forthcoming experiments,[1] Therefore, here we will discuss the peculiarities of ESSνSB and the differences from other experiments in the determination of the oscillation parameters before presenting our numerical results. The ν_e appearance oscillation probability in matter is given by [27] (see also [74–76]):

$$\begin{aligned} P(\overset{(-)}{\nu}_\mu \to \overset{(-)}{\nu}_e) = {} & s^2_{23} \sin^2 2\theta_{13} \left(\frac{\Delta_{31}}{\tilde{B}_\mp}\right)^2 \sin^2\left(\frac{\tilde{B}_\mp L}{2}\right) + c^2_{23} \sin^2 2\theta_{12} \left(\frac{\Delta_{21}}{A}\right)^2 \sin^2\left(\frac{AL}{2}\right) \\ & + \tilde{J} \frac{\Delta_{21}}{A} \frac{\Delta_{31}}{\tilde{B}_\mp} \sin\left(\frac{AL}{2}\right) \sin\left(\frac{\tilde{B}_\mp L}{2}\right) \left[\cos\delta \cos\left(\frac{\Delta_{31} L}{2}\right) \mp \sin\delta \sin\left(\frac{\Delta_{31} L}{2}\right)\right], \end{aligned} \tag{2.1}$$

where $\Delta_{ij} \equiv \Delta m^2_{ij}/2E$, $\tilde{J} = c_{13} \sin 2\theta_{12} \sin 2\theta_{23} \sin 2\theta_{13}$, $A = \sqrt{2} G_F n_e$ is the matter potential with n_e the electron density and G_F the Fermi constant, and $\tilde{B}_\mp \equiv |A \mp \Delta_{13}|$. In this expression the only dependence in the CP violating phase δ appears in the last term, which is the interference between the "atmospheric" oscillation in the first term and the "solar" in the second. Since $\sin 2\theta_{13} \sim 0.3$ while $\Delta_{12} L \sim 0.05$ at the first oscillation peak, the "atmospheric" term tends to dominate the oscillation probability and the interesting CP interference is only subleading. Conversely, at the second oscillation maximum $\Delta_{12} L \sim 0.1$ so that the dependence on δ of the oscillation probability is much higher which allows to improve the sensitivity to this parameter [28]. This can be seen in Fig. 1 where the change in the probability upon changing the values of δ is much more significant at the second peak maximum compared to the first.

[1] The MOMENT proposal [59–62] with $L = 150$ km can access to the oscillation probability with similar L/E to the ESSνSB. The T2HKK proposal [63–73], in which the first and the second oscillation maxima are measured with two detectors located at different sites, would also cover the similar L/E range to the ESSνSB.

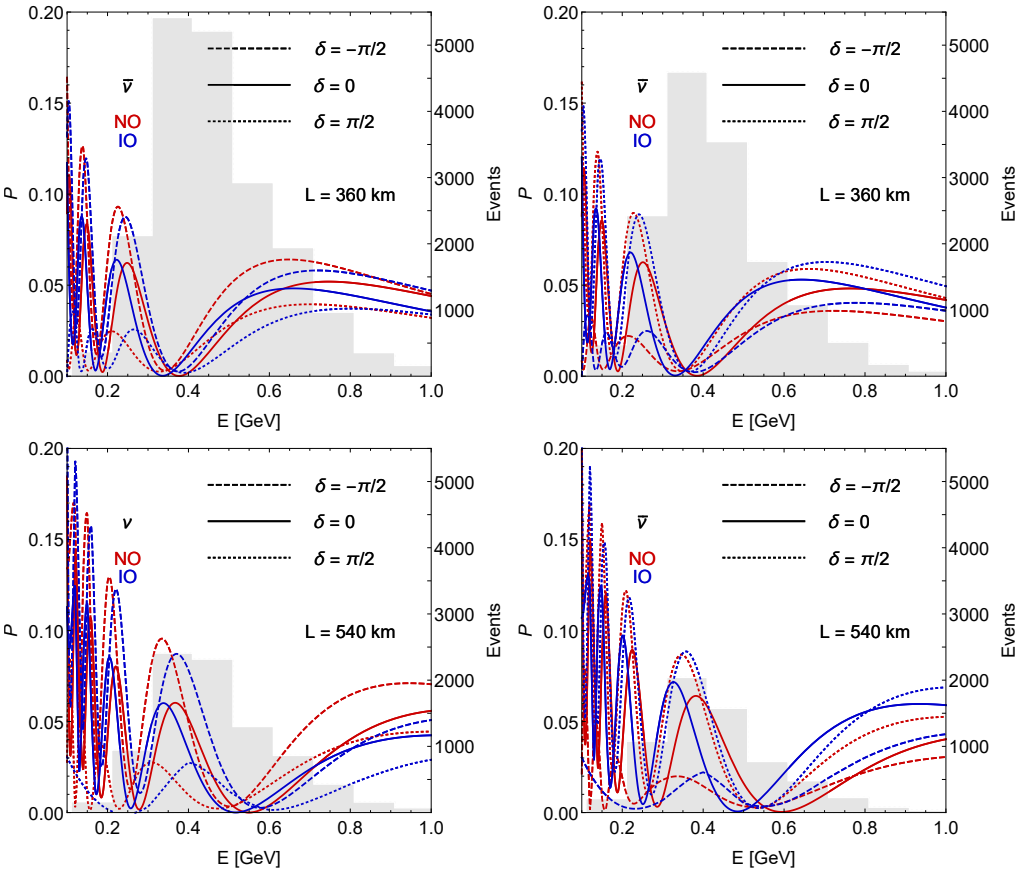


Figure 1: Oscillation probabilities for the Zinkgruvan (upper panels) and Garpenberg (lower panels) baselines as a function of the energy for neutrinos (left panels) and antineutrinos (right panels). The red (blue) lines are for normal (inverted) ordering and three different values of $\delta = -\pi/2$, 0 and $\pi/2$ are represented by the dashed, solid and dotted lines respectively. The grey histograms show the number of events that would be obtained in each energy bin for a 2/8 time splitting between neutrino/antineutrino mode if the oscillation probability was 1. Thus, they serve as a guide of what energies of the oscillation probability would be well-sampled by the ESSνSB setup.

In Eq. (2.1) the leading dependence on the mass ordering comes from the "atmospheric" term, as it goes as the inverse of the square of $\tilde{B}_{\mp}$. For $E \sim |\Delta m^2_{31}|/(2A)$ there will be a resonance which will produce an enhancement in neutrinos against antineutrinos or viceversa depending on the mass ordering. For a typical average matter density of 3.0 g/cm^3 one finds that the approximate energy for this resonance to happen is $E \sim \mathcal{O}$(GeV). Given that the peak of the flux for ESSνSB happens at $E \sim \mathcal{O}(100)$ MeV (see Fig. 1), the importance of the matter effects and hence of the sensitivity to the mass ordering for this facility is not expected to be significant.

The bi-probability plots [31] shown in Fig. 2 help to illustrate the degeneracy problem at the ESSνSB experiment. Here all oscillation parameters other than δ, the octant of θ_{23}, and the sign of Δm^2_{31} are fixed at the current best fit values [24], and the matter density along the neutrino baseline is assumed to be constant with an average density of 3.0 g/cm^3. The baseline length L and the neutrino energies E are set to $L = 540$ km (ESS-Garpenberg)

and $E = \{280, 380, 480\}$ MeV. The ellipses show the variation of the appearance probabilities for the neutrino and antineutrino channels from changes in δ. The four ellipses in each plot correspond to the different choices of the octant of θ_{23} and the mass ordering. When the ellipses overlap sharing the same region in the $P(\nu_\mu \to \nu_e)$-$P(\bar{\nu}_\mu \to \bar{\nu}_e)$ plane, the same oscillation probabilities can be obtained by changing δ, the octant of θ_{23} and/or the mass ordering, implying the existence of degenerate solutions.

Let us first focus on the middle plot with $E = 380$ MeV where the oscillation probabilities are close to the second maximum, $|\Delta m^2_{31}|L/(4E) \sim 3\pi/2$. The centres of the ellipses are located on the CP conserving line $P(\nu_\mu \to \nu_e) = P(\bar{\nu}_\mu \to \bar{\nu}_e)$, which reflects the fact that the matter effect, which could induce an explicit difference between the neutrino and antineutrino oscillation probabilities unrelated to the intrinsic CP violation from δ, is irrelevant for this energy and baseline. The major axes of the ellipses extend widely along the diagonal line orthogonal to the CP conserving line. This means that the CP violating term proportional to $\sin\delta$ in Eq.(2.1) is very relevant in the oscillation probability for this energy and baseline, leading to the improved CP sensitivity at the second oscillation peak.

The "fake" CP violation effect due to the matter effect separates the two ellipses with opposite mass ordering at the first oscillation maximum, where T2HK focuses on, causing the δ-sign(Δm^2_{31}) degeneracy in the CP violation search, cf. the right most plot in Fig. 3. Conversely, the CP violation search at the second oscillation maximum is not noticeably affected by the matter effect [30, 77]. Changing the value of θ_{23}, the ellipses almost keep the same shape and move in parallel along the CP conserving line, which causes the δ-θ_{23} degeneracy [36, 37].

The vertices of the ellipses are located at $\delta = \{\pi/2, -\pi/2\}$, where the oscillation probabilities do not change much with a change of δ. As a consequence, the precision in the determination of δ becomes worse close to the oscillation maxima [78]. In other words, since the two points with δ and $\pi - \delta$ on an ellipse are close to each other around $\delta = \{\pi/2, -\pi/2\}$, it is hard to separate them [78]. Although at the probability level from Fig. 2 the expectation would be that this quasi-degeneracy effect occurs similarly at $\delta = \pi/2$ and $\delta = -\pi/2$, the numerical simulations we will report in Section 4 show that the ESSνSB suffers this effect more severely at $\delta = -\pi/2$ than at $\delta = \pi/2$. This is due to the significant difference in event rates between these two points. Indeed, for $\delta = -\pi/2$, the oscillation probability for neutrinos is enhanced while the antineutrino one is suppressed. Since both the flux and the cross section are also smaller for antineutrinos, this strongly penalizes the measurement at $\delta = -\pi/2$ since the antineutrino sample is essentially lost given that the event rate at the second oscillation peak is already necessarily small. On the other hand, at $\delta = \pi/2$, the oscillation probability for neutrinos is suppressed, but the larger cross section and flux compensate for it and prevents such a big loss of sensitivity.

In the energy region that the ESSνSB focuses on, the oscillation phase changes rapidly. As a consequence, the shape and location of the ellipses changes very significantly even within the same energy bin. In Fig. 2, we also show the bi-probability plots with E =280 and 480 MeV where the oscillation probabilities are approaching the minima, which are also well-covered by the ESSνSB flux. The ellipses are not distributed symmetrically to the CP conserving line, which means that, contrary to the second peak, matter effects do have some impact on the oscillation probabilities. However, this impact is still subleading, given the rather low energy, and does not shift the energies where the extrema are located, cf. Fig. 1. As a result, the two ellipses for the different mass hierarchies are not separated in the entire energy region.

The drastic shape change of the ellipses when varying the energy is largely due to the

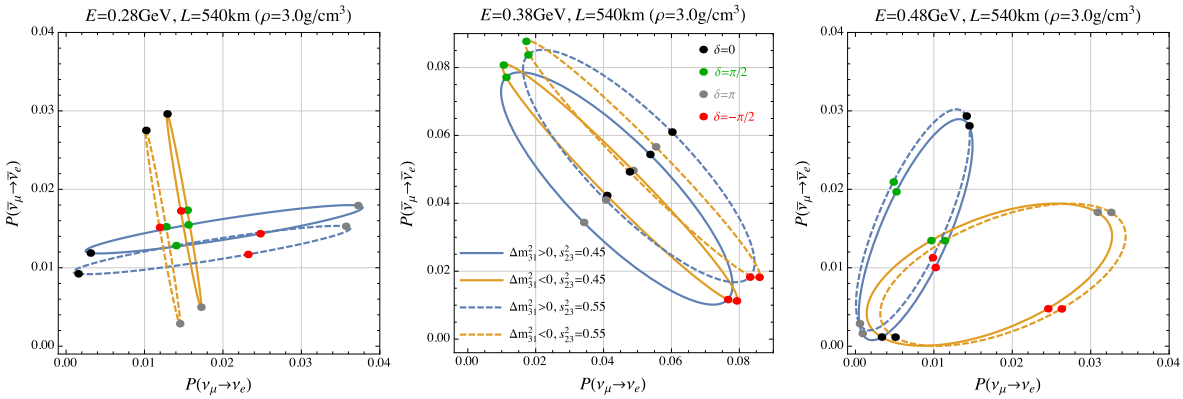


Figure 2: Bi-probability plots for the ESS-Garpenberg setup $L = 540$ km. Three plots for three different neutrino energies: $E = \{280, 380, 480\}$ MeV from left to right. The four ellipses in each plot for the different choices of $(s^2_{23} \equiv \sin^2\theta_{23}, \text{sign}[\Delta m^2_{31}])$: blue solid for $(0.45, +)$, orange solid for $(0.45, -)$, blue dashed for $(0.55, +)$, and orange dashed for $(0.55, -)$. The energies $E = 380$ MeV and $E = 480$ MeV correspond to the vicinity of the second oscillation maximum and the first oscillation minimum.

ratio of the $\sin\delta$ and the $\cos\delta$ terms in the oscillation probability, see Eq. (2.1). The $\sin\delta$ term is most significant close to the oscillation peak with $|\Delta m^2_{31}|L/(4E) \simeq 3\pi/2$ for $E \simeq 380$ MeV. As the probabilities depart from the maximum, the major axes of the ellipses start following along the direction of the CP conserving line, which means that the $\cos\delta$ term increases in importance as we approach the minima with $|\Delta m^2_{31}|L/(4E) \simeq \pi$ (right panel of Fig. 2) or $|\Delta m^2_{31}|L/(4E) \simeq 2\pi$ (left panel). In the left and the right plots, the ellipses with different mass orderings intersect each other at points with different values of δ at different energies. Therefore, in principle, with precise enough measurements at various energies, one could determine the value of δ and the sign of Δm^2_{31} separately. However, the oscillations are too fast for the ~ 100 MeV resolution achievable at these energies with a water Cerenkov detector to resolve and also the event rate at the second maximum is not large enough to perform a very fine binning. Thus, it is not possible to track the rapid oscillations in Fig. 1, although some mild sensitivity to the mass ordering can be achievable.

A large overlap between the two ellipses with different mass orderings and different octants at the oscillation maximum (middle panel in Fig. 2), where most of the statistics is concentrated, suggests that the mass ordering sensitivity at the beam experiment is affected by the octant degeneracy.

The ellipses for different octants barely separate in the entire energy region, which implies a rather poor sensitivity to θ_{23} in the appearance channel leading to octant degeneracies that can spoil both the determination of δ and of the mass ordering at the ESSνSB. Conversely, for experiments focusing on the first maxium the two ellipses for different octants are more separated [30], cf. the right panel in Fig. 3. Therefore, we will explore the impact of the addition of the atmospheric neutrino data collected at the far detector of the ESSνSB to the beam data since atmospheric neutrinos can provide both sensitivity to the θ_{23} octant and the mass ordering helping to lift parametric degeneracies [32, 33].

The mass ordering sensitivity from an observation of atmospheric neutrinos comes from the oscillation signals driven by Δm^2_{31} and the matter effect (first term in Eq. (2.1)) and therefore, it does not depend on the value of δ. On the other hand, the sensitivity is better

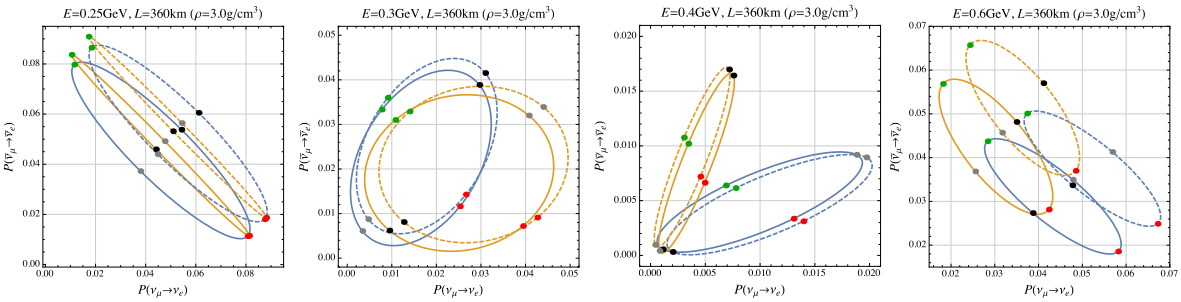


Figure 3: Bi-probability plots for $L = 360$ km (ESS-Zinkgruvan). In this energy range $E = 250 - 600$ MeV, the oscillation probabilities experience the second maximum, the first minimum, and the first maximum.

for θ_{23} in the second octant than the first octant, since the term is proportional to $\sin^2\theta_{23}$ [79].

If the shorter baseline $L = 360$ km (ESS-Zinkgruvan) is instead considered, the neutrino flux at the high energy tail up to $E \sim 600$ MeV covers the first oscillation maximum. This situation corresponds to the bi-probability ellipses presented in the right panel of Fig. 3, which show the same shape and position characteristic of other experiments located at the first oscillation maximum such as T2HK. The matter effect is not significant enough to completely separate the two mass orderings. In the relevant energy range (200-600 MeV), the oscillation probabilities go from the first maximum (right panel) to the first minimum (middle panels) and to the second maximum (left panel). The leftmost panel with $E = 250$ MeV, where the second oscillation peak would be located, looks very similar to that with $E = 380$ MeV in the case of $L = 540$ km. The ellipses for the different mass orderings are separated more clearly in the case of $L = 360$ km than $L = 540$ km in a large energy region, which leads to a slightly better sensitivity to the mass ordering even though the baseline is shorter. From the information at the first oscillation maximum, the ESSνSB with $L = 360$ km also has better sensitivity to θ_{23} than the $L = 540$ km option, so that it is expected that the longer baseline option will benefit more from the addition of the atmospheric neutrino data, which helps to determine θ_{23} and its octant.

3 Simulation and experimental details

The simulation of the ESSνSB data has been performed with the GLoBES software [80, 81]. We have assumed that the neutrino beam will shine on a near and a far detector to reduce the systematic uncertainties [18]. The far detector is a 1 Mt MEMPHYS-like water Cerenkov detector [20], while the near detector has been assumed to be identical to the far detector in terms of efficiencies and background rejection capabilities with a fiducial mass of 0.1 kt. The response of the detectors has been implemented through migration matrices, both for the signal efficiency and the background rejection from Ref. [20].

A beam power of 5 MW with 2.5 GeV protons and an exposure of 1.7×10^7 operating seconds per year has been assumed [18]. The fluxes have been simulated explicitly at 1 km for the near detector [82], accounting for possible geometrical effects since the source cannot be considered point-like, as well as for 100 km (and consequently rescaled) for the longer baselines considered for the far detector [18]. The event rate peaks around $\mathcal{O}(100)$ MeV energies (see Fig.1), so the dominant contribution to the cross section will be in the quasi-elastic regime

Systematics	Opt.	Cons.
Fiducial volume ND	0.2%	0.5%
Fiducial volume FD	1%	2.5%
Flux error ν	5%	7.5%
Flux error $\bar{\nu}$	10%	15%
Neutral current background	5%	7.5%
Cross section $\times$ eff. QE	10%	15%
Ratio ν_e/ν_μ QE	3.5%	11%

Table 1: Systematic uncertainties for a super beam as described in Ref. [39] for two different scenarios, the "Optimistic" one and the "Conservative" scenario where systematics are larger.

(QE). For the cross section we use the results from the Genie [83] tune G18_10a_00_000.

We have assumed a total running time of 10 years. Nonetheless, we will also study the dependence of the physics reach on the relative running time spent in positive and negative focusing in order to optimize it for the measurement of CP violation. Likewise, although the preferred location of the far detector for the ESSνSB is the Garpenberg mine at 540 km [18], different baselines, with emphasis in the alternative Zinkgruvan option at 360 km, will be studied to address the optimal choice. Finally, we will also study how the CP discovery potential depends on the total exposure.

Throughout all the simulations we adopt the same treatment of the systematic errors from Table 1 as in Ref. [39]. Unless otherwise specified, we will assume the "Optimistic" systematics from the first "Opt." column in Table 1 although we will also show how the results are affected when the more conservative ones in the second column "Cons." are considered instead. All systematics have been introduced as nuisance parameters and the results presented have been obtained minimizing the χ^2 over all of them. The systematic uncertainties associated to fluxes and cross sections have been assumed to be fully correlated between near and far detector and uncorrelated between neutrino and antineutrino components and different flavours. The uncertainties on the fiducial volumes of the near and far detectors were not assumed to be correlated. Additionally, to account for the uncertainty in the cross section between the near and far detector, arising from the different flavour composition of the beam (mainly ν_μ in the near site and ν_e for the signal in the far detector), a completely uncorrelated systematic is included for their ratio (last row of Table 1). Therefore, the χ^2 will be given by

$$\chi^2 = \min_{n_{s_i}} \left(\hat{\chi}^2_{FD}[n_{s_C}] + \hat{\chi}^2_{ND}[n_{s_C}, n_{s_U}] + \frac{n^2_{s_C}}{\sigma^2_{n_{s_C}}} + \frac{n^2_{s_U}}{\sigma^2_{n_{s_U}}} \right), \tag{3.1}$$

where $\hat{\chi}^2_{FD}$ ($\hat{\chi}^2_{ND}$) corresponds to the far (near) detector and n_{s_C} (n_{s_U}) are the correlated (uncorrelated) systematic uncertainties.

We have added to the resulting χ^2 a gaussian prior with the central values and 1σ errors from Ref. [24] for "solar" and "reactor" parameters. For the "atmospheric" parameters we set a prior on $\sin^2 2\theta_{23}$ and $|\Delta m^2_{31}|$ given that the octant for θ_{23} and the mass ordering are still unknown. Since the determination of these two parameters comes primarily from atmospherics, when adding this sample to the beam data no prior has been added on θ_{23} and Δm^2_{31}.

The simulation of the atmospheric neutrino sample in MEMPHYS is the one used in the analysis from Ref. [33] where the neutrino fluxes at Gran Sasso from Honda calculations [84]

were used. This is a conservative estimate as fluxes become larger at higher geomagnetic latitudes such as Garpenberg or Zinkgruvan. In the simulation the events are separated between fully and partially contained events in the detector and stopping from through-going muon events. The neutral current contamination in each bin was included assuming the same ratio as Super-Kamiokande between neutral-current and unoscillated charged-current events [85]. For further details on the atmospheric sample see [33].

4 Results

In Fig. 4 we show the impact on the CP discovery potential of the ESSνSB before (dashed lines) and after (solid lines) the inclusion of the atmospheric sample for the Zinkgruvan (360 km) and Garpenberg (540 km) options in the left and right panels, respectively. The plots represent the $\sqrt{\Delta\chi^2}$ with which CP conserving values of $\delta = 0$ or π can be disfavoured as a function of the true value of δ. We take the minimum of $\Delta\chi^2$ between $\delta = 0$ and π. The $\sqrt{\Delta\chi^2}$ can be interpreted as the significance for exclusion of CP-conserving values (and hence evidence for CP violation) as long as the assumptions behind Wilks' theorem hold [86]. Deviations from these assumptions can be sizable for presently running experiments, but are expected to be smaller for next generation facilities [87].

Even though the sensitivity of the atmospheric neutrino dataset to δ is almost negligible, the improvement of the ESSνSB physics reach upon its inclusion is quite remarkable. The improvement is generally larger for the longer 540 km baseline than for the Zinkgruvan 360 km option. This is in line with the expectations discussed in Section 2 of the atmospheric sample being more complementary to the beam information at the longer baseline. Indeed, at the second oscillation maximum the ν_μ disappearance oscillation is not sampled as efficiently as at the first peak and this deteriorates the determination of the atmospheric oscillation parameters θ_{23} and Δm^2_{31}, which play an important role in the measurement of δ. Conversely, the 360 km baseline has higher statistics and some events also cover the first oscillation maximum such that the atmospheric oscillation information is less complementary and the gain upon its inclusion is less noticeable. From these results we can conclude that the ESSνSB setup combined with the atmospheric neutrino sample would be able to rule out CP-conserving values of δ for $\sim 60\%$ ($\sim 55\%$) of the possible values of δ at the 5σ level regardless of the octant and the mass ordering when observing at the 540 km (360 km) baseline.

Figure 4 also shows that the gain in CP discovery potential is much more pronounced in some particular regions of the parameter space, especially for $\delta < 0$ and θ_{23} in the first octant or $\delta > 0$ and the second octant. In these examples the dotted curves for beam only often show a kink that reduces the slope and the values of δ for which CP-violation could be discovered with high significance. Conversely, the corresponding solid curves with atmospheric data either do not display the kink or develop it at higher significance so that the resulting CP-discovery potential is much larger. These kinks occur due to the presence of an unresolved octant degeneracy at a CP-conserving value of δ that prevents drawing conclusions regarding CP violation. When atmospheric data is added, the sensitivity to the octant improves and these degeneracies are either lifted or only show up at much higher significance.

This situation is illustrated in Fig. 5, where the allowed regions at the $\Delta\chi^2 = 25$ level are shown in the δ-$\sin^2\theta_{23}$ plane. The left (right) panels assume the true values $\delta = -40^\circ$ ($\delta = 150^\circ$), $\sin^2 2\theta_{23} = 0.418$ ($\sin^2 2\theta_{23} = 0.582$) and normal ordering. As can be seen, when only the beam information is taken into account (blue curves), an octant degeneracy that spreads

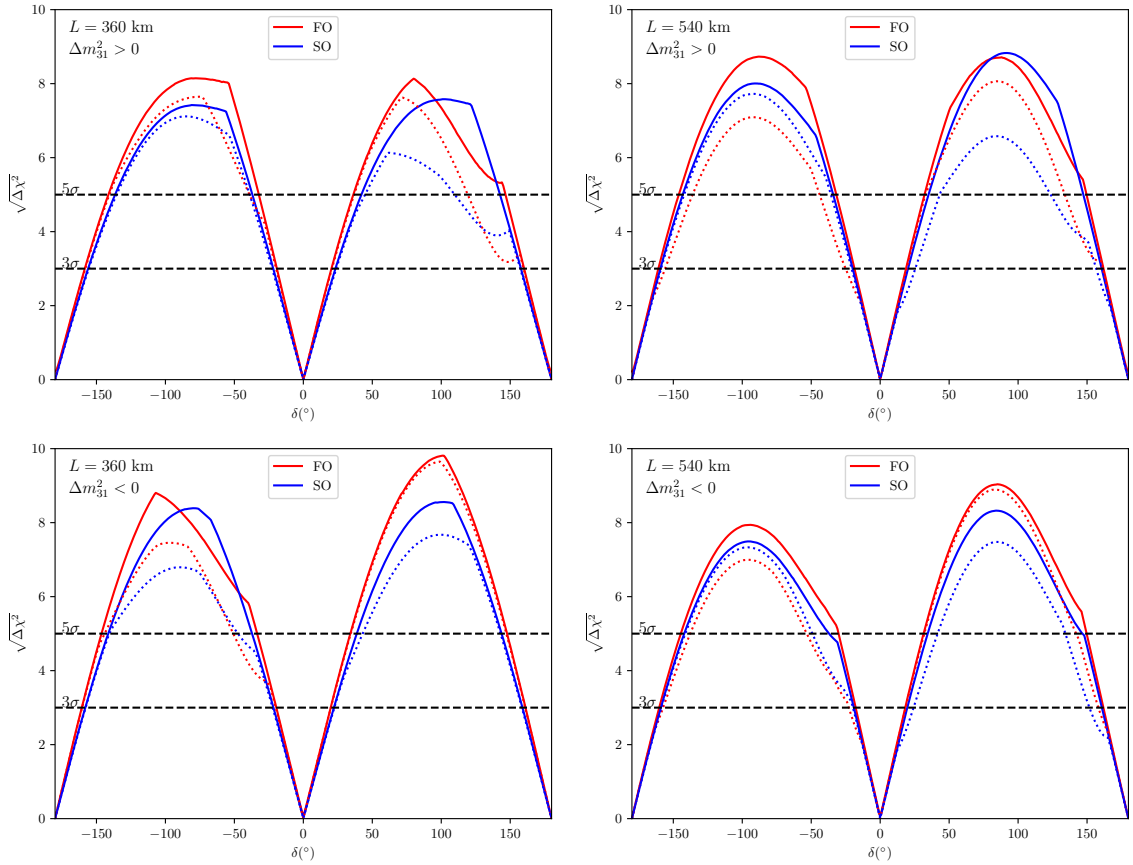


Figure 4: Significance with which CP conserving values of δ can be excluded for the Zinkgruvan 360 km (left panels) and Garpenberg 540 km (right panels) options. The upper (lower) plots are for normal (inverted) mass ordering while the red (blue) curves correspond to θ_{23} in the first (second) octant. The dashed lines correspond to the beam data only, while the continuous lines correspond to the results studying events from the beam and from atmospheric neutrinos. The running time splitting has been assumed to be t_ν=$t_{\bar{\nu}} = 5$ years.

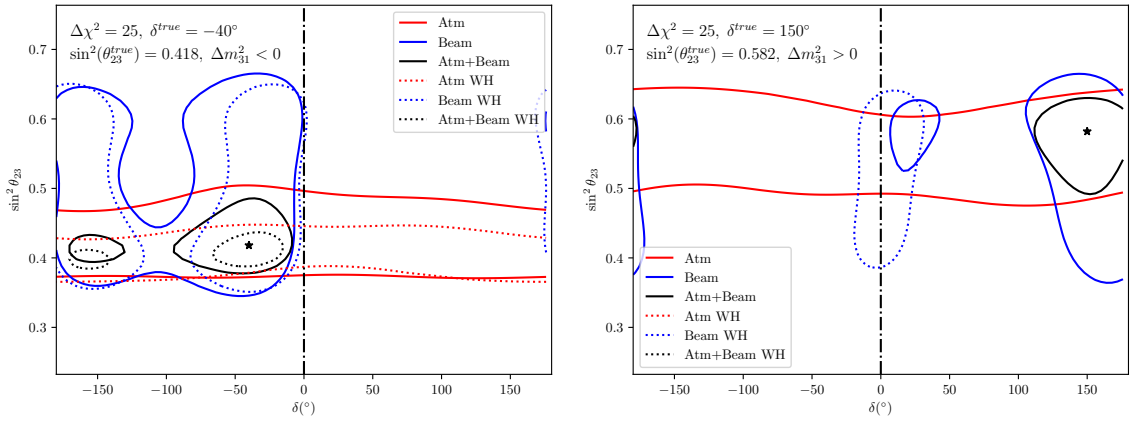


Figure 5: Allowed regions at $\Delta\chi^2 = 25$ for different assumed values of $\sin^2\theta_{23}$ and δ represented by the star for a 540 km baseline (Garpenberg location). The red curves correspond to the atmospheric dataset alone, the blue to the beam-only information and the black curves to the combination of both. Dotted regions are allowed with the wrong mass ordering. The running time splitting has been assumed to be t_ν=$t_{\bar{\nu}} = 5$ years.

the allowed region towards CP conserving values appears. Conversely, the atmospheric data on their own (red curves) have no capability to determine δ at all, but can instead rule out the wrong octant of θ_{23}. Thus, the combination of the two data sets (black curves) very significantly improves the CP discovery potential of the facility in these areas of parameter space. The dotted lines correspond to "sign" degeneracies with the opposite mass ordering to the one chosen as true value. In the right panel this degeneracy is also solved with atmospheric data while for the values of δ and θ_{23} chosen in the left panel a small sign degeneracy remains between the 4 and 5σ level. Notice that an "intrinsic degeneracy" [34] at $\delta \simeq \pi - \delta_{true}$ also shows up at the 5σ level when only the beam information is taken into account. As for the "sign" degeneracy, the atmospheric neutrino data is enough to lift it for the parameters chosen in the right panel while a small remnant is present in the left. In any case, both the "intrinsic" and the "sign" degeneracies appear at $\delta \simeq \pi - \delta_{true}$, given the comparatively small matter effects for the setup, and their allowed regions are smaller or comparable to that of the true solution so that only the "octant"degeneracy plays a significant role in reducing the CP-discovery potential when atmospheric data is not exploited to lift it.

In Fig. 6 we show how the significance with which the ESSνSB would be able to disfavour the wrong octant of θ_{23} as a function of the true value of θ_{23} (blue lines). As already anticipated in Section 2, this capability improves dramatically upon the inclusion of the atmospheric neutrino sample (red lines) and thus the potentially dangerous "octant" degeneracies are lifted. The curves are almost identical for both mass orderings and for the Zinkgruvan and Garpenberg baselines.

The significance with which the ESSνSB would be able to disfavour the wrong mass ordering is shown in Fig. 7, where dotted (solid) lines correspond to beam only data (beam and atmospheric data). The left (right) panels correspond to the 360 km (540 km) baseline and upper (lower) panels are for the scenario in which the true ordering is normal (inverted). As can be seen the ESSνSB beam data allows to disfavour the wrong mass ordering at around the 3σ (2σ) level for the 360 km (540 km) baseline for any value of δ and the octant. When the atmospheric data is added, the sensitivity to the wrong ordering is boosted to the 4-5σ level or

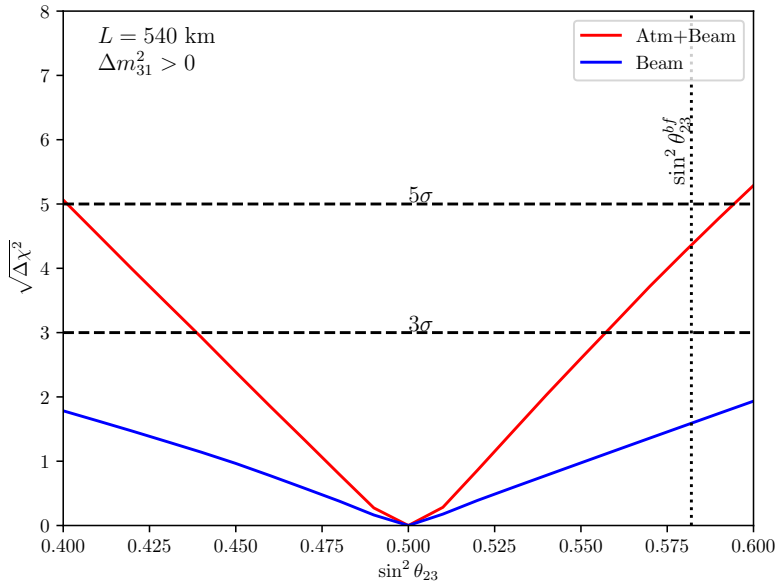


Figure 6: Significance with which the wrong octant would be disfavoured as a function of the actual value of θ_{23} with beam-only information (blue lines) and including also the atmospheric dataset (red lines) for the baseline to Garpenberg ($L = 540$ km) and normal mass ordering. The running time splitting has been assumed to be t_ν=$t_{\bar{\nu}} = 5$ years. The results for the Zinkgruvan site ($L = 360$ km) and for inverted ordering are very similar. The vertical line represents the present best fit for θ_{23} from [24].

even higher for the particular case of normal ordering and second octant of θ_{23} ($\sin^2\theta_{23} = 0.582$ from Ref. [24]) for which the signal in atmospheric neutrinos is enhanced, as expected from Eq.(2.1). For normal ordering (upper panels) the inclusion of the atmospheric neutrino data also change the shape of the curve, in particular a larger increase in the significance is seen around $\delta = 0$ than for other values. This is due to the solution of the octant degeneracy since, as can be seen in the middle panel of Fig. 2 or the first panel of Fig. 3, for $\delta = 0$ and normal ordering the ellipse with opposite octant and ordering has a significant overlap.

In Fig. 8 we analyze the precision with which the ESSνSB experiment would be able to measure the CP-violating phase δ. In this figure we assumed the currently preferred option of normal ordering and second octant of θ_{23}. In the upper panels we show the improvement in the 1σ allowed region with which δ would be constrained by adding the atmospheric neutrino sample (solid lines) to the beam information alone (dotted lines). As can be seen, both for the 360 km (left panel) and 540 km baseline (right panel), the precision with which δ could be determined has a very pronounced shape. For CP violating values of δ around $\pm 90°$, the 1σ uncertainty in the measurement peaks leading to the poorest precision, while for δ around 0 or 180° the most precise measurements would be achieved.

As discussed in Ref. [78], this structure follows from the dependence of the oscillation probability on δ shown in Eq.(2.1). At an oscillation peak $|\Delta m^2_{31}|L/(4E) = (2n-1)\pi/2$ and thus mainly $\sin\delta$ is probed. Since the derivative of $\sin\delta$ vanishes at $\delta = \pm 90°$, the precision with which δ can be determined is worst close to these values. In order to constrain δ around $\delta = \pm 90°$, measurements away from the oscillation maxima to determine $\cos\delta$ would instead be necessary. These off-peak measurements are easier at the Zinkgruvan 360 km baseline since

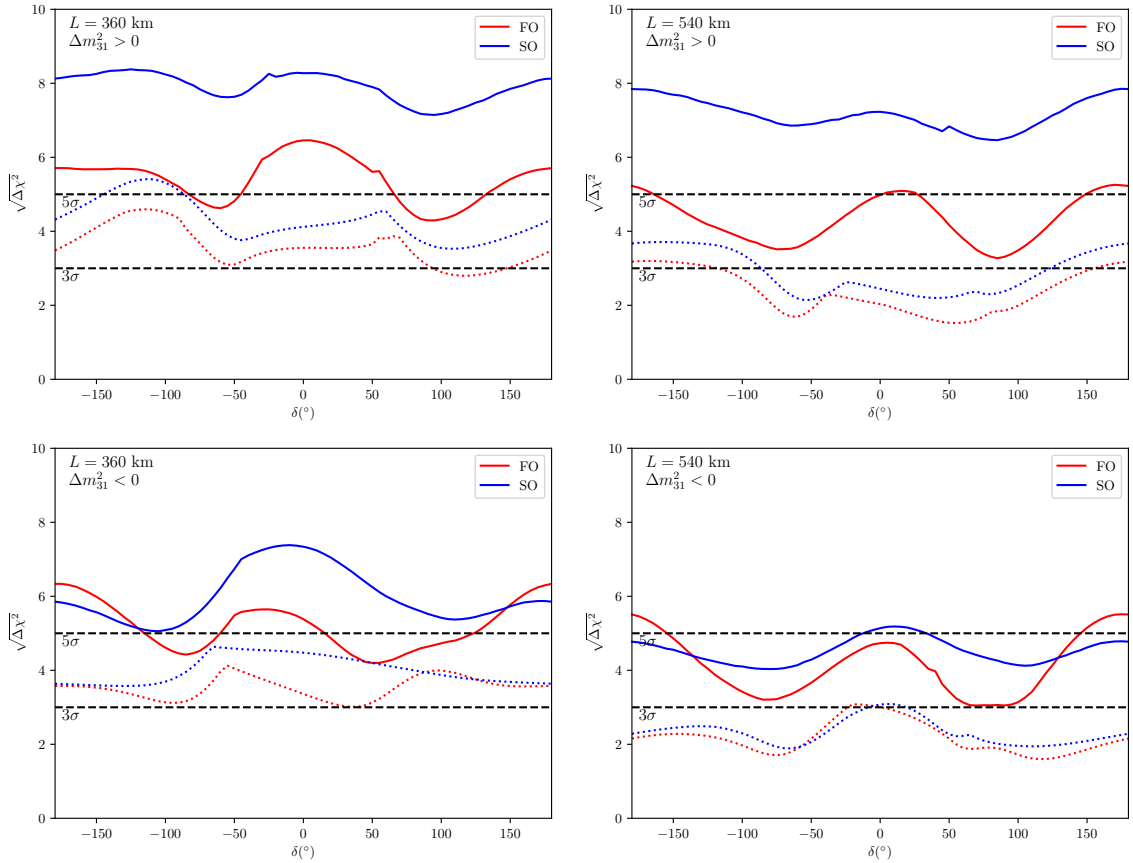


Figure 7: Significance with which the wrong mass ordering would be disfavoured for θ_{23} in the first octant (red lines) or second octant (blue lines) and the true mass ordering being normal (upper plots) or inverted (lower plots). Dashed lines correspond to the beam only data while solid lines correspond to the addition of the atmospheric sample. The left panels correspond to the baseline to Zinkgruvan while the right ones to the location of the Garpenberg mine. The running time has been assumed to be $t_\nu{=}t_{\bar{\nu}} = 5$ years.

the statistics is higher and also the beam is not exactly centered at the maximum, while they are very challenging at Garpenberg since very few events away from the oscillation peak are expected. This explains why the reconstructed sensitivities around $\delta = \pm 90°$ are much worse in the right panel compared to the left. Moreover, the double-peak structure that can be seen for $\delta = -90°$ for 540 km corresponds to the "intrinsic" degeneracies depicted in Fig. 5 that merge into one bigger allowed region. Since, as seen in Fig. 5, the addition of atmospheric data can lift these degeneracies, in the solid lines where this information was included the difference between the two baselines is significantly reduced.

Conversely, for $\delta = 0$ or $180°$ the measurement on peak is what allows to determine δ and, since this is better covered at the longer 540 km baseline, the precision is slightly better there. This fact also translates into the better CP-discovery potential observed for the 540 km baseline in Fig. 4. Since the error in δ is smaller around CP-conserving values, the 540 km option could get closer to these values but still allow to claim the discovery of CP violation with high significance.

In the lower panels of Fig. 8, the impact of changing the relative running times in positive

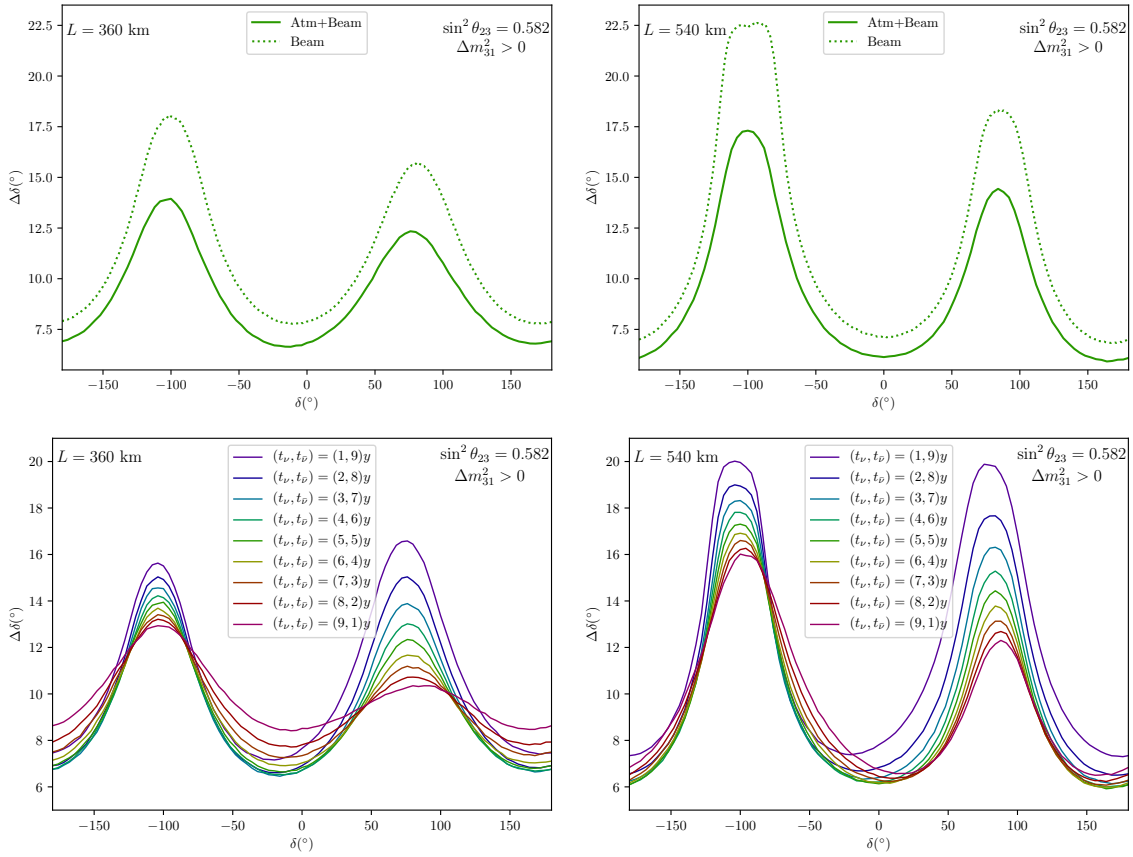


Figure 8: Precision (spread of the 1σ allowed region) on the determination of δ for the baseline to Zinkgruvan $L = 360$ km (left panels) and Garpenberg $L = 540$ km (right panels) for the current best-fit parameters [24]. In the upper panels we show the comparison between the precision obtained with (solid lines) and without (dashed lines) the atmospheric sample for a running time of 5 years in each focusing. In the lower plots we show the dependence of the precision on the relative running time in each mode, where t_ν ($t_{\bar{\nu}}$) corresponds to the time the experiment would run in neutrino (antineutrino) mode, combining atmospheric and beam datasets.

focusing (neutrino mode) and negative focusing (antineutrino mode) is shown. Since off-peak measurements are required for $\delta = \pm 90°$, statistics are crucial and easier to accumulate in neutrino mode, since fluxes and cross sections are larger, and thus the best precision would be obtained by devoting longer periods of data taking to positive focusing. Conversely, around $\delta = 0$ or $180°$ the complementarity between the neutrino and antineutrino samples pays off and more even splits of the running time provide better sensitivity.

Since the ESSνSB would be a next-generation facility, its measurement strategy can profit from the previous hints by preceding oscillation experiments and adapt the splitting between neutrino and antineutrino modes depending on what value of δ data point to. If such a strategy is followed and the best splitting between neutrino and antineutrino modes is adopted for each value of δ, the precision presented in Fig. 9 would be obtained. If the mass ordering is confirmed to be normal and θ_{23} lies in the second octant as present data prefer, the precision with which the ESSνSB facility would determine δ ranges from $16°$ ($13°$) for $\delta \sim -90°$ to $6°$

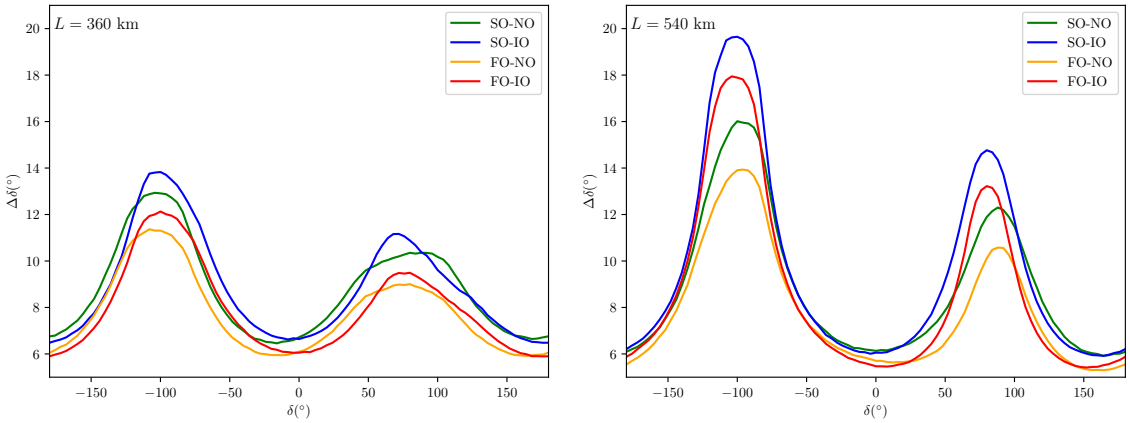


Figure 9: Precision on the measurement of δ for a total running time of 10 years when the relative running time in neutrino and antineutrino modes is optimized for each value of δ. This corresponds to running similar times in neutrino and antineutrino modes around $\delta = 0, 180°$ and maximizing the neutrino runs around $\delta = \pm 90°$.

(7°) for $\delta \sim 0$ or $\delta \sim 180°$ for 540 km (360 km).

From Figs. 4 and 9 one can conclude that if the experiments preceding the ESSνSB do not find any evidence for CP-violation, the best option would be the 540 km baseline and a more or less even split of the neutrino and antineutrino running times. Indeed, this choice would minimize the errors with which δ would be determined around CP-conserving values and allow to increase the CP-discovery potential. On the other hand, if the previous set of experiments determine δ to be close to maximally CP-violating, then the best scenario for the ESSνSB would be the shorter 360 km baseline and increased neutrino run time to determine δ with the best precision possible.

In Fig. 10 we show the impact of individual systematic uncertainties on the fraction of values of δ for which CP violation could be discovered ($\Delta\chi^2 \geq 25$). The sources of uncertainty considered, summarized in Table 1, are the flux uncertainties for the signal ($\delta\phi_S$) and background ($\delta\phi_B$), the cross section systematic ($\delta\sigma$), the neutral current background (δNC_B), and the uncertainty on the ratio of the electron and muon flavour neutrino cross section ($\delta\sigma_e/\sigma_\mu$). The plot shows that the systematic uncertainties that most significantly affect the performance of the ESSνSB are the ones related to the background components of the beam, since for these the determination at the near detector is more challenging. Namely, $\delta\phi_B$, δNC_B as well as $\delta\sigma_e/\sigma_\mu$ since the only ν_e present at the near detector that would allow to fix this parameter are those from the intrinsic background contamination of the beam. Among these, the strongest impact on the sensitivity is due to the cross section ratio since, not only it is difficult to constrain, but it is also most relevant to the signal at the far detector, which consists of ν_e. Indeed, reducing or increasing this particular source of systematic error has the biggest impact on the physics reach. The impact is in any event limited, since the main bottleneck to the performance when observing at the second oscillation peak is statistics. In particular, a reduction of this systematic by a factor of 5 improves the CP fraction by $\sim 2\%$ (no impact for $\bar{\nu}$) while the same factor in the opposite direction worsens the sensitivity by $\sim 9\%$ ($\sim 4\%$).

The importance of these systematic errors in the physics reach is crucially dependent on the baseline of the experiment. In the left panel of Fig. 11 we show the fraction of all the possible

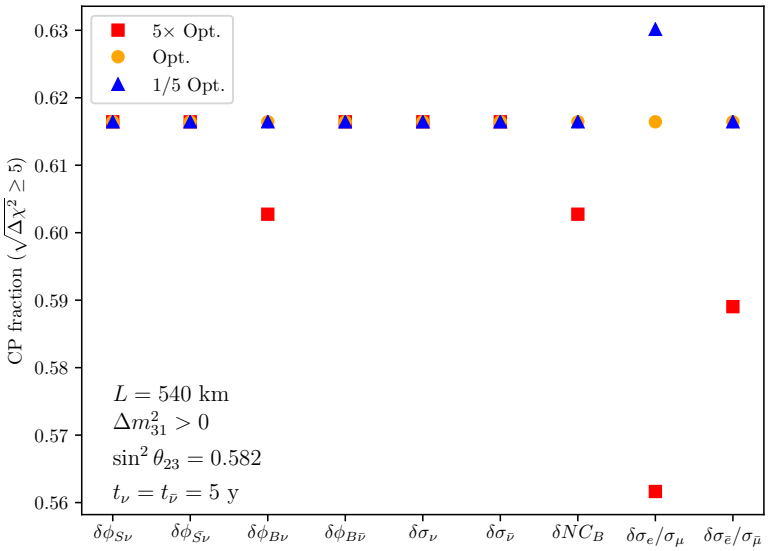


Figure 10: Impact of different sources of systematic errors on the fraction of values of δ for which a $\Delta\chi^2 > 25$ exclusion of CP conservation would be possible at the Garpenberg mine. The orange circles correspond to the CP fraction with the "Optimistic" systematics from Table 1, red squares correspond to assuming that particular uncertainty to be 5 times larger and blue triangles to reducing the uncertainty by a factor of 5.

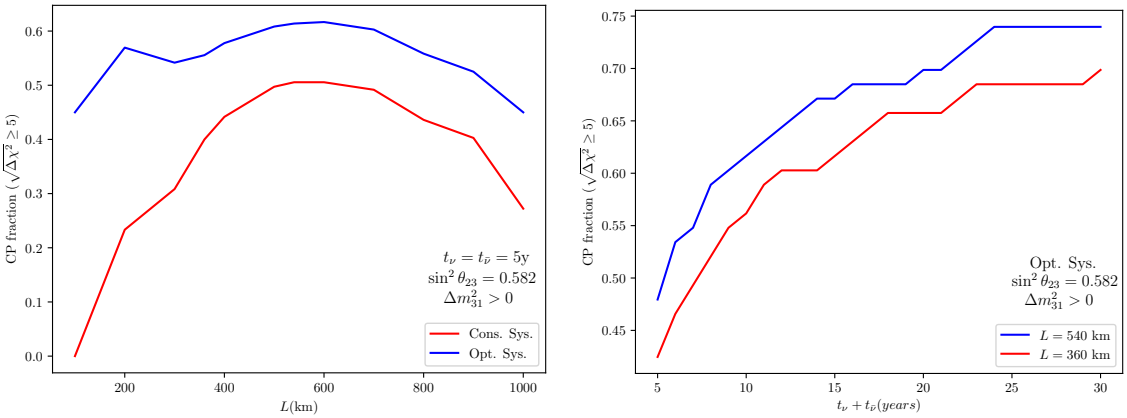


Figure 11: Fraction of values of δ for which CP violation could be discovered above 5σ for different baselines to the far detector (left panel) for the two different sets of systematics from Table 1. In the right panel we show the CP fraction for the Garpenberg ($L = 540$ km) and Zinkgruvan ($L = 360$ km) mines, assuming the current best fit values for the oscillation parameters and the "Optimistic" systematics for increasing total exposure.

values of δ for which it would be possible to rule out $\delta = 0$ or $\delta = 180^\circ$ with a $\Delta\chi^2 = 25$ or higher significance. The upper blue line is for the more optimistic systematics from Table 1 and the lower red one for the more conservative values. As can be seen, the fraction of values of δ at which a 5σ discovery would be possible, peaks between 400 km and 700 km in both cases. But this peak is much more pronounced when the more conservative values are assumed for the systematic uncertainties. Indeed, for larger values of the systematics, the shorter baselines are strongly penalized since the dependence of the oscillation probability is subleading around the first peak and easily hidden by the systematics. Conversely, if very small systematic errors can be achieved, then the main limiting factor would be statistics and shorter baselines would perform better. Thus, by measuring at the second oscillation maximum the ESSνSB setup becomes much more resilient to sources of systematic errors unaccounted for than when observing only at the first peak.

In the right panel of Fig. 11 we show how the fraction of values of δ for which CP violation would be discovered at the 5σ level by the ESSνSB beam and atmospheric data increases with the exposure. As expected from an observation at the second oscillation peak, statistics is the main factor controlling the final reach of the experiment. Indeed, for 5 years data taking the CP fraction is around 46%, by 10 years it increases to 62% and reaches 70% for 20 years of exposure. The slope only flattens significantly after 25 years.

5 Conclusions

In this paper we have performed an exhaustive analysis of the physics reach of the ESSνSB facility exploring its capability to determine all the presently unknown neutrino oscillation parameters such as the mass ordering and the octant of θ_{23} but with a focus on the discovery of leptonic CP violation and a precision measurement of δ, which are the main declared goals of the experiment. For the first time we combined the atmospheric neutrino sample that would also be observed at the facility with the beam information and studied the complementarity between the two data sets. We studied how the physics reach of the facility could be optimized by exploring different baselines and focusing on the two candidate sites of Zinkgruvan at 360 km and Garpenberg at 540 km. We have also explored how the time split between neutrino and antineutrino modes can be exploited to improve the physics reach.

We conclude that the inclusion of the atmospheric data set can significantly increase the ESSνSB physics reach. Due to the peculiarities of observing the oscillation probability at the second oscillation maximum we find that this combination is particularly synergistic. The atmospheric neutrino sample not only significantly increases the sensitivity to the mass ordering, like for other similar facilities [32, 33], but it is also very effective in improving the constraints on Δm^2_{31} and θ_{23} and its octant. These measurements are especially challenging for the beam alone when sitting at the second maximum, given the low statistics, particularly in antineutrinos and in the ν_μ disappearance channel. However, the determination of δ can be affected by correlations with θ_{23} [37] and degeneracies with the wrong octant and thus the atmospheric information is also crucial to increase the CP discovery potential of the ESSνSB indirectly. We find this complementarity is somewhat more pronounced for the longer 540 km baseline since there the flux is more centered at the second oscillation peak and the statistics are smaller so it benefits more from the information gained from the atmospheric neutrino data.

Regarding the optimal baseline, we find the choice is rather dependent of the actual value

of δ. For $\delta \sim \pm 90^\circ$ a precise measurement needs events away from the oscillation maximum. In this sense the shorter 360 km baseline is better since the statistics for off-peak events are higher and this leads to a more precise measurement. Conversely, if δ is close to CP conserving values and the previous set of measurements have not been able to claim the discovery of CP-violation, the longer 540 km baseline would allow to cover a larger part of the parameter space. Indeed, after 10 years of data taking, the fraction of values of δ for which a 5σ discovery would be possible is 56% for Zinkgruvan and 62% for Garpenberg.

As for the splitting of the data taking time between neutrino and antineutrino modes, the optimal strategy also depends on the value of δ. This fact could be exploited since previous and present data at the time of the measurement should already show a strong preference for some part of the parameter space. Thus, the running strategy can be adapted to the situation optimizing the precision with which this measurement can be performed. In particular we find again that given the need of going beyond measurements at the peak for $\delta \sim \pm 90^\circ$, statistics is much more relevant and maximizing the time in neutrino mode translates to the best precision for these values. Conversely, close to CP-conserving values of δ, the information from events on-peak is most relevant and the complementarity between neutrino and antineutrino modes pays off so that a more even split of the running time would provide the best precision.

Finally we explored the possible bottlenecks for the physics reach of the facility exploring how it is affected by varying the values of the different systematic errors considered as well as the total exposure. As expected, the choice of observing the oscillation probability at its second maximum significantly reduces the impact of the systematic errors. We find that around the first oscillation peak the fraction of values of δ for which a 5σ discovery is possible is reduced by more than a factor 2 when considering the more conservative values of Table 1. On the other hand, at the second peak the reduction is only by a factor around 1.2. Among the different sources of systematic uncertainties considered, the most important is the possible difference in the ratio of the electron to muon neutrino cross sections. This uncertainty is difficult to constrain from near detector information since the flux is mainly composed of ν_μ, but the far detector signal consists of ν_e. Conversely, the observation at the second maximum considerably reduces the number of events and statistics play a much more relevant role. At the longer 540 km baseline, the fraction of values of δ allowing for a discovery would go from 47% to 62% and 70% for data taking periods of 5, 10, and 20 years, respectively.

Acknowledgements

We are extremely grateful to Michele Maltoni for providing us with the simulations of atmospheric neutrino dataset that would be collected at the MEMPHYS detector used in Ref. [33]. We are also indebted to Budimir Klicek and Marco Roda for suggestions and help with the GENIE tunes most appropriate for the ESSνSB energy range. We also want to thank WP6 of the ESSνSB design study, in particular Monojit Ghosh, for comments on our manuscript. f This work is supported in part by the European Union's Horizon 2020 research and innovation programme under the Marie Sklodowska-Curie grant agreements 674896-Elusives, 690575-InvisiblesPlus, and 777419-ESSnuSB, as well as by the COST Action CA15139 EuroNuNet. MB, EFM, and SR acknowledge support from the "Spanish Agencia Estatal de Investigación" (AEI) and the EU "Fondo Europeo de Desarrollo Regional" (FEDER) through the project FPA2016-78645-P; and the Spanish MINECO through the "Ramón y Cajal" programme and through the Centro de Excelencia Severo Ochoa Program under grant SEV-2016-0597. MB

also acknowledges support from the Göran Gustafsson foundation.

References

[1] DAYA-BAY Collaboration Collaboration, F. An et al., *Observation of electron-antineutrino disappearance at Daya Bay*, *Phys.Rev.Lett.* **108** (2012) 171803 [arXiv:1203.1669].

[2] RENO collaboration Collaboration, J. Ahn et al., *Observation of Reactor Electron Antineutrino Disappearance in the RENO Experiment*, *Phys.Rev.Lett.* **108** (2012) 191802 [arXiv:1204.0626].

[3] Double Chooz Collaboration Collaboration, Y. Abe et al., *Reactor electron antineutrino disappearance in the Double Chooz experiment*, *Phys.Rev.* **D86** (2012) 052008 [arXiv:1207.6632].

[4] MINOS Collaboration Collaboration, P. Adamson et al., *Improved search for muon-neutrino to electron-neutrino oscillations in MINOS*, *Phys.Rev.Lett.* **107** (2011) 181802 [arXiv:1108.0015].

[5] T2K Collaboration Collaboration, K. Abe et al., *Indication of Electron Neutrino Appearance from an Accelerator-produced Off-axis Muon Neutrino Beam*, *Phys.Rev.Lett.* **107** (2011) 041801 [arXiv:1106.2822].

[6] B. Pontecorvo, *Mesonium and anti-mesonium*, *Sov.Phys.JETP* **6** (1957) 429.

[7] B. Pontecorvo, *Inverse beta processes and nonconservation of lepton charge*, *Sov.Phys.JETP* **7** (1958) 172–173.

[8] Z. Maki, M. Nakagawa, Y. Ohnuki and S. Sakata, *A unified model for elementary particles*, *Prog.Theor.Phys.* **23** (1960) 1174–1180.

[9] Z. Maki, M. Nakagawa and S. Sakata, *Remarks on the unified model of elementary particles*, *Prog.Theor.Phys.* **28** (1962) 870–880.

[10] B. Pontecorvo, *Neutrino Experiments and the Problem of Conservation of Leptonic Charge*, *Sov.Phys.JETP* **26** (1968) 984–988.

[11] T2K Collaboration, K. Abe et al., *Combined Analysis of Neutrino and Antineutrino Oscillations at T2K*, *Phys. Rev. Lett.* **118** (2017) 151801 [arXiv:1701.00432].

[12] T2K Collaboration, K. Abe et al., *Constraint on the Matter-Antimatter Symmetry-Violating Phase in Neutrino Oscillations*, arXiv:1910.03887.

[13] NOvA Collaboration, M. A. Acero et al., *First Measurement of Neutrino Oscillation Parameters using Neutrinos and Antineutrinos by NOvA*, arXiv:1906.04907.

[14] M. Gavela, P. Hernandez, J. Orloff and O. Pene, *Standard model CP violation and baryon asymmetry*, *Mod.Phys.Lett.* **A9** (1994) 795–810 [arXiv:hep-ph/9312215].

[15] M. Gavela, P. Hernandez, J. Orloff, O. Pene and C. Quimbay, *Standard model CP violation and baryon asymmetry. Part 2: Finite temperature*, *Nucl.Phys.* **B430** (1994) 382–426 [arXiv:hep-ph/9406289].

[16] Hyper-Kamiokande Proto-Collaboration Collaboration, K. Abe et al., *Physics potential of a long-baseline neutrino oscillation experiment using a J-PARC neutrino beam and Hyper-Kamiokande*, *PTEP* **2015** (2015) 053C02 [arXiv:1502.05199].

[17] DUNE Collaboration, R. Acciarri et al., *Long-Baseline Neutrino Facility (LBNF) and Deep Underground Neutrino Experiment (DUNE)*, arXiv:1512.06148.

[18] ESSnuSB Collaboration, E. Baussan et al., *A very intense neutrino super beam experiment for leptonic CP violation discovery based on the European spallation source linac*, *Nucl. Phys.* **B885** (2014) 127–149 [arXiv:1309.7022].

[19] A. de Bellefon et al., *MEMPHYS: A Large scale water Cerenkov detector at Frejus*, arXiv:hep-ex/0607026.

[20] MEMPHYS Collaboration, L. Agostino, M. Buizza-Avanzini, M. Dracos, D. Duchesneau, M. Marafini, M. Mezzetto et al., *Study of the performance of a large scale water-Cherenkov detector (MEMPHYS)*, *JCAP* **1301** (2013) 024 [arXiv:1206.6665].

[21] S. K. Agarwalla, S. Choubey and S. Prakash, *Probing Neutrino Oscillation Parameters using High Power Superbeam from ESS*, *JHEP* **12** (2014) 020 [arXiv:1406.2219].

[22] K. Chakraborty, K. N. Deepthi and S. Goswami, *Spotlighting the sensitivities of Hyper-Kamiokande, DUNE and ESS ? SB*, *Nucl. Phys.* **B937** (2018) 303–332 [arXiv:1711.11107].

[23] K. Chakraborty, S. Goswami, C. Gupta and T. Thakore, *Enhancing the hierarchy and octant sensitivity of ESSνSB in conjunction with T2K, NOνA and ICAL@INO*, *JHEP* **05** (2019) 137 [arXiv:1902.02963].

[24] I. Esteban, M. C. Gonzalez-Garcia, A. Hernandez-Cabezudo, M. Maltoni and T. Schwetz, *Global analysis of three-flavour neutrino oscillations: synergies and tensions in the determination of $\theta_2 3, \delta_C P$, and the mass ordering*, *JHEP* **01** (2019) 106 [arXiv:1811.05487].

[25] Daya Bay Collaboration, D. Adey et al., *Measurement of the Electron Antineutrino Oscillation with 1958 Days of Operation at Daya Bay*, *Phys. Rev. Lett.* **121** (2018) 241805 [arXiv:1809.02261].

[26] RENO Collaboration, G. Bak et al., *Measurement of Reactor Antineutrino Oscillation Amplitude and Frequency at RENO*, *Phys. Rev. Lett.* **121** (2018) 201801 [arXiv:1806.00248].

[27] A. Cervera, A. Donini, M. B. Gavela, J. J. Gomez Cadenas, P. Hernandez, O. Mena et al., *Golden measurements at a neutrino factory*, *Nucl. Phys.* **B579** (2000) 17–55 [arXiv:hep-ph/0002108].

[28] P. Coloma and E. Fernandez-Martinez, *Optimization of neutrino oscillation facilities for large θ_{13}*, *JHEP* **04** (2012) 089 [arXiv:1110.4583].

[29] G. L. Fogli and E. Lisi, *Tests of three flavor mixing in long baseline neutrino oscillation experiments*, *Phys. Rev.* **D54** (1996) 3667–3670 [arXiv:hep-ph/9604415].

[30] M. Ghosh and T. Ohlsson, *A comparative study between ESSnuSB and T2HK in determining the leptonic CP phase*, arXiv:1906.05779.

[31] H. Minakata and H. Nunokawa, *Exploring neutrino mixing with low-energy superbeams*, *JHEP* **10** (2001) 001 [arXiv:hep-ph/0108085].

[32] P. Huber, M. Maltoni and T. Schwetz, *Resolving parameter degeneracies in long-baseline experiments by atmospheric neutrino data*, *Phys. Rev.* **D71** (2005) 053006 [arXiv:hep-ph/0501037].

[33] J.-E. Campagne, M. Maltoni, M. Mezzetto and T. Schwetz, *Physics potential of the CERN-MEMPHYS neutrino oscillation project*, *JHEP* **04** (2007) 003 [arXiv:hep-ph/0603172].

[34] J. Burguet-Castell, M. B. Gavela, J. J. Gomez-Cadenas, P. Hernandez and O. Mena, *On the Measurement of leptonic CP violation*, *Nucl. Phys.* **B608** (2001) 301–318 [arXiv:hep-ph/0103258].

[35] V. Barger, D. Marfatia and K. Whisnant, *Breaking eight fold degeneracies in neutrino CP violation, mixing, and mass hierarchy*, *Phys. Rev.* **D65** (2002) 073023 [arXiv:hep-ph/0112119].

[36] H. Minakata and S. J. Parke, *Correlated, precision measurements of θ_{23} and δ using only the electron neutrino appearance experiments*, *Phys. Rev.* **D87** (2013) 113005 [arXiv:1303.6178].

[37] P. Coloma, H. Minakata and S. J. Parke, *Interplay between appearance and disappearance channels for precision measurements of θ_{23} and δ*, *Phys. Rev.* **D90** (2014) 093003 [arXiv:1406.2551].

[38] M. Ghosh, P. Ghoshal, S. Goswami, N. Nath and S. K. Raut, *New look at the degeneracies in the neutrino oscillation parameters, and their resolution by T2K, NOνA and ICAL*, *Phys. Rev.* **D93** (2016) 013013 [arXiv:1504.06283].

[39] P. Coloma, P. Huber, J. Kopp and W. Winter, *Systematic uncertainties in long-baseline neutrino oscillations for large θ_{13}*, *Phys. Rev.* **D87** (2013) 033004 [arXiv:1209.5973].

[40] S. C, K. N. Deepthi and R. Mohanta, *A comprehensive study of the discovery potential of NOvA, T2K and T2HK experiments*, *Adv. High Energy Phys.* **2016** (2016) 9139402 [arXiv:1408.6071].

[41] M. Ghosh, S. Goswami and S. K. Raut, *Maximizing the DUNE early physics output with current experiments*, *Eur. Phys. J.* **C76** (2016) 114 [arXiv:1412.1744].

[42] Hyper-Kamiokande Working Group Collaboration, K. Abe et al., *A Long Baseline Neutrino Oscillation Experiment Using J-PARC Neutrino Beam and Hyper-Kamiokande*, 2014 [arXiv:1412.4673].

[43] M. Ghosh and O. Yasuda, *Effect of systematics in the T2HK, T2HKK, and DUNE experiments*, *Phys. Rev.* **D96** (2017) 013001 [arXiv:1702.06482].

[44] Hyper-Kamiokande Collaboration, K. Abe et al., *Hyper-Kamiokande Design Report*, arXiv:1805.04163.

[45] LBNE Collaboration, C. Adams et al., *The Long-Baseline Neutrino Experiment: Exploring Fundamental Symmetries of the Universe*, in *Snowmass 2013: Workshop on Energy Frontier Seattle, USA, June 30-July 3, 2013*, 2013 [arXiv:1307.7335].

[46] V. Barger, A. Bhattacharya, A. Chatterjee, R. Gandhi, D. Marfatia and M. Masud, *Configuring the Long-Baseline Neutrino Experiment*, *Phys. Rev.* **D89** (2014) 011302 [arXiv:1307.2519].

[47] M. Ghosh, P. Ghoshal, S. Goswami and S. K. Raut, *Synergies between neutrino oscillation experiments: an 'adequate' configuration for LBNO*, *JHEP* **03** (2014) 094 [arXiv:1308.5979].

[48] LAGUNA-LBNO Collaboration, S. K. Agarwalla et al., *The mass-hierarchy and CP-violation discovery reach of the LBNO long-baseline neutrino experiment*, *JHEP* **05** (2014) 094 [arXiv:1312.6520].

[49] V. Barger, A. Bhattacharya, A. Chatterjee, R. Gandhi, D. Marfatia and M. Masud, *Optimal configurations of the Deep Underground Neutrino Experiment*, *Int. J. Mod. Phys.* **A31** (2016) 1650020 [arXiv:1405.1054].

[50] K. Bora, D. Dutta and P. Ghoshal, *Determining the octant of θ_{23} at LBNE in conjunction with reactor experiments*, *Mod. Phys. Lett.* **A30** (2015) 1550066 [arXiv:1405.7482].

[51] N. Nath, M. Ghosh and S. Goswami, *The physics of antineutrinos in DUNE and determination of octant and δ_{CP}*, *Nucl. Phys.* **B913** (2016) 381–404 [arXiv:1511.07496].

[52] V. De Romeri, E. Fernandez-Martinez and M. Sorel, *Neutrino oscillations at DUNE with improved energy reconstruction*, *JHEP* **09** (2016) 030 [arXiv:1607.00293].

[53] DUNE Collaboration, B. Abi et al., *The DUNE Far Detector Interim Design Report Volume 1: Physics, Technology and Strategies*, arXiv:1807.10334.

[54] A. De GouvÃ^{a}a, K. J. Kelly, G. V. Stenico and P. Pasquini, *Physics with Beam Tau-Neutrino Appearance at DUNE*, *Phys. Rev.* **D100** (2019) 016004 [arXiv:1904.07265].

[55] A. Ghoshal, A. Giarnetti and D. Meloni, *On the role of the $\nu_?$ appearance in DUNE in constraining standard neutrino physics and beyond*, *JHEP* **12** (2019) 126 [arXiv:1906.06212].

[56] D. Meloni, *On the systematic uncertainties in DUNE and their role in New Physics studies*, *JHEP* **08** (2018) 028 [arXiv:1805.01747].

[57] S. Fukasawa, M. Ghosh and O. Yasuda, *Complementarity Between Hyperkamiokande and DUNE in Determining Neutrino Oscillation Parameters*, *Nucl. Phys.* **B918** (2017) 337–357 [arXiv:1607.03758].

[58] P. Ballett, S. F. King, S. Pascoli, N. W. Prouse and T. Wang, *Sensitivities and synergies of DUNE and T2HK*, *Phys. Rev.* **D96** (2017) 033003 [arXiv:1612.07275].

[59] J. Cao et al., *Muon-decay medium-baseline neutrino beam facility*, *Phys. Rev. ST Accel. Beams* **17** (2014) 090101 [arXiv:1401.8125].

[60] M. Blennow, P. Coloma and E. Fernández-Martinez, *The MOMENT to search for CP violation*, *JHEP* **03** (2016) 197 [arXiv:1511.02859].

[61] P. Bakhti and Y. Farzan, *CP-Violation and Non-Standard Interactions at the MOMENT*, *JHEP* **07** (2016) 109 [arXiv:1602.07099].

[62] J. Tang, S. Vihonen and T.-C. Wang, *Precision measurements on δ_{CP} in MOMENT*, *JHEP* **12** (2019) 130 [arXiv:1909.01548].

[63] M. Ishitsuka, T. Kajita, H. Minakata and H. Nunokawa, *Resolving neutrino mass hierarchy and CP degeneracy by two identical detectors with different baselines*, *Phys. Rev.* **D72** (2005) 033003 [arXiv:hep-ph/0504026].

[64] K. Hagiwara, N. Okamura and K.-i. Senda, *Solving the neutrino parameter degeneracy by measuring the T2K off-axis beam in Korea*, *Phys. Lett.* **B637** (2006) 266–273 [arXiv:hep-ph/0504061].

[65] K. Hagiwara, N. Okamura and K.-i. Senda, *Physics potential of T2KK: An Extension of the T2K neutrino oscillation experiment with a far detector in Korea*, *Phys. Rev.* **D76** (2007) 093002 [arXiv:hep-ph/0607255].

[66] T. Kajita, H. Minakata, S. Nakayama and H. Nunokawa, *Resolving eight-fold neutrino parameter degeneracy by two identical detectors with different baselines*, *Phys. Rev.* **D75** (2007) 013006 [arXiv:hep-ph/0609286].

[67] K. Hagiwara and N. Okamura, *Solving the degeneracy of the lepton-flavor mixing angle theta(ATM) by the T2KK two detector neutrino oscillation experiment*, *JHEP* **01** (2008) 022 [arXiv:hep-ph/0611058].

[68] K. Hagiwara and N. Okamura, *Re-evaluation of the T2KK physics potential with simulations including backgrounds*, *JHEP* **07** (2009) 031 [arXiv:0901.1517].

[69] K. Hagiwara, N. Okamura and K.-i. Senda, *The earth matter effects in neutrino oscillation experiments from Tokai to Kamioka and Korea*, *JHEP* **09** (2011) 082 [arXiv:1107.5857].

[70] K. Hagiwara, T. Kiwanami, N. Okamura and K.-i. Senda, *Physics potential of neutrino oscillation experiment with a far detector in Oki Island along the T2K baseline*, *JHEP* **06** (2013) 036 [arXiv:1209.2763].

[71] K. Hagiwara, P. Ko, N. Okamura and Y. Takaesu, *Revisiting T2KK and T2KO physics potential and ν_μ - $\bar{\nu}_\mu$ beam ratio*, *Eur. Phys. J.* **C77** (2017) 138 [arXiv:1605.02368].

[72] Hyper-Kamiokande Collaboration, K. Abe et al., *Physics potentials with the second Hyper-Kamiokande detector in Korea*, *PTEP* **2018** (2018) 063C01 [arXiv:1611.06118].

[73] S. K. Raut, *Matter effects at the T2HK and T2HKK experiments*, *Phys. Rev.* **D96** (2017) 075029 [arXiv:1703.07136].

[74] M. Freund, M. Lindner, S. T. Petcov and A. Romanino, *Testing matter effects in very long baseline neutrino oscillation experiments*, *Nucl. Phys.* **B578** (2000) 27–57 [arXiv:hep-ph/9912457].

[75] E. K. Akhmedov, R. Johansson, M. Lindner, T. Ohlsson and T. Schwetz, *Series expansions for three flavor neutrino oscillation probabilities in matter*, *JHEP* **04** (2004) 078 [arXiv:hep-ph/0402175].

[76] H. Minakata and S. J. Parke, *Simple and Compact Expressions for Neutrino Oscillation Probabilities in Matter*, *JHEP* **01** (2016) 180 [arXiv:1505.01826].

[77] J. Bernabeuu and A. Segarra, *Signatures of the genuine and matter-induced components of the CP violation asymmetry in neutrino oscillations*, *JHEP* **11** (2018) 063 [arXiv:1807.11879].

[78] P. Coloma, A. Donini, E. Fernandez-Martinez and P. Hernandez, *Precision on leptonic mixing parameters at future neutrino oscillation experiments*, *JHEP* **06** (2012) 073 [arXiv:1203.5651].

[79] E. K. Akhmedov, S. Razzaque and A. Yu. Smirnov, *Mass hierarchy, 2-3 mixing and CP-phase with Huge Atmospheric Neutrino Detectors*, *JHEP* **02** (2013) 082 [arXiv:1205.7071].

[80] P. Huber, M. Lindner and W. Winter, *Simulation of long-baseline neutrino oscillation experiments with GLoBES (General Long Baseline Experiment Simulator)*, *Comput. Phys. Commun.* **167** (2005) 195 [arXiv:hep-ph/0407333].

[81] P. Huber, J. Kopp, M. Lindner, M. Rolinec and W. Winter, *New features in the simulation of neutrino oscillation experiments with GLoBES 3.0: General Long Baseline Experiment Simulator*, *Comput. Phys. Commun.* **177** (2007) 432–438 [arXiv:hep-ph/0701187].

[82] M. Blennow, P. Coloma and E. Fernandez-Martinez, *Searching for sterile neutrinos at the ESSνSB*, *JHEP* **12** (2014) 120 [arXiv:1407.1317].

[83] C. Andreopoulos, C. Barry, S. Dytman, H. Gallagher, T. Golan, R. Hatcher et al., *The GENIE Neutrino Monte Carlo Generator: Physics and User Manual*, arXiv:1510.05494.

[84] M. Honda, T. Kajita, K. Kasahara and S. Midorikawa, *A New calculation of the atmospheric neutrino flux in a 3-dimensional scheme*, *Phys. Rev.* **D70** (2004) 043008 [arXiv:astro-ph/0404457].

[85] Super-Kamiokande Collaboration, Y. Ashie et al., *A Measurement of atmospheric neutrino oscillation parameters by SUPER-KAMIOKANDE I*, *Phys. Rev.* **D71** (2005) 112005 [arXiv:hep-ex/0501064].

[86] S. S. Wilks, *The Large-Sample Distribution of the Likelihood Ratio for Testing Composite Hypotheses*, *Annals Math. Statist.* **9** (1938) 60–62.

[87] M. Blennow, P. Coloma and E. Fernandez-Martinez, *Reassessing the sensitivity to leptonic CP violation*, *JHEP* **03** (2015) 005 [arXiv:1407.3274].